Observation of Kes 27:
A Typical Mixed-Morphology SNR

Hideyuki Enoguchi, Hiroshi Tsunemi, Emi Miyata, and Kumi Yoshita

Department of Earth and Space Science, Graduate School of Science, Osaka University,

1-1 Machikaneyama, Toyonaka, Osaka 560-0043

enoguchi@ess.sci.osaka-u.ac.jp, tsunemi@ess.sci.osaka-u.ac.jp,

miyata@ess.sci.osaka-u.ac.jp, kyoshita@ess.sci.osaka-u.ac.jp

Abstract

We report here on the observation of Kes 27, a proto-typical mixed-morphology SNR, using ASCA. It clearly shows a filled-center structure in the X-ray region while a shell structure in the radio region. There are two radio bright regions: one is in the center, while the other is in the east rim. The X-ray intensity peak coincides well with the radio bright region at the center. The X-ray spectrum was well-fitted by a collisional ionization equilibrium model with solar abundances. Taking into account the ionization parameter ($>10^{12}$ cm^{-3}s) and the plasma density ($0.39^{+0.03}_{-0.02}$ cm^{-3}), we found that the age of the SNR is longer than 8×10^4 yr. The hardness ratio map indicates that the inner region shows a harder spectrum than that in the outer region, which does not come from the heavier interstellar absorption feature, but from the higher temperature. There is a temperature gradient from the innner region (0.84 ± 0.08 keV) toward outer region ($0.59^{+0.04}_{-0.06}$ keV), indicating that the thermal conduction does not play an important role.

Key words: ISM: abundances — ISM: individual (Kes 27) — supernova remnants — X-rays: ISM)

1. Introduction

There are two types of Supernova remnants (SNRs) in the X-ray region from a morphological point of view: a shell structure and a filled-center structure. Some SNRs in each type contain a point source at its center. Therefore, the point source at its center does not always affect the morphology of the SNR. The shell structure is generated as the result of a blast wave propagating inside the interstellar matter (ISM), while the origin of the filled-center structure has not yet been established. A cloud evaporation model can explain the filled-center structure (White, Long 1991). The clouds in the interstellar space will gradually evaporate after passage

of the blast wave, which enhances the brightness of the central part of the SNR, resulting in the filled-center structure. Many of them show evidence of the interactions with molecular clouds, and have been studied from a theoretical point of view (Chevalier 1999). Another explanation is a radiative phase model (Cox 1972). When the density at the shell region increases, the radiative instability proceeds and reduces the temperature of the shell region so that it becomes X-ray dim in the shell region.

Rho and Petre (1998) proposed a new group of SNR, "mixed-morphology (MM) SNR", among the filled-center SNRs based on a ROSAT observation. They are characterized as having 1) a shell structure in the radio region, 2) a filled-center structure in the X-ray region, 3)an absence of a compact source in its center, and 4) thin thermal emission in the X-ray region showing a solar or sub-solar abundance. The forth criterion is considered to mean that the X-ray emitting plasma is not contaminated by the ejecta. They selected 7 SNRs belonging to this group as proto-typical MM SNRs: W 28, W 44, 3C 400.2, Kes 27, MSH 11-61A, 3C 391 and CTB 1. They also claimed 7 other SNRs as probably belonging to this group.

In young SNRs, like Cassiopeia-A, there is a large inhomogeneity in metal abundance (Hwang et al. 2000). Even in a middle-aged SNR, like the Cygnus Loop, the abundance in the shell region is quite different from that in its center (Miyata et al. 1998, 1999), whereas the absolute intensity in the center is quite weak. Although these two SNRs belong to the shell structure, it will take long time before the convection of the ejecta with the ISM is completed. Therefore, the uniform abundance in the SNR may become an important clue to form a new class of SNRs.

Among the MM SNRs, Yoshita et al. (2001) reported on the X-ray structure of 3C 400.2 using the ASCA satellite, which has better energy resolution than that of ROSAT. They found no spectral variation across the SNR, with a possible exception of the abundance of Fe. Due to an elongation in the radio image, they studied a possible interaction of two SNRs. They concluded that it was generated from a single SNR, rather than two.

The SNR, Kes 27 (G327.4+0.4), is classified as a proto-typical MM type SNR. In the radio wavelength, it shows a shell structure with a diameter of $\sim 20'$ with a slight complexity, a typical shell with an arm in the northwest. It has a spectral index of $\alpha = 0.6 \pm 0.05$ where $S_\nu \sim \nu^{-\alpha}$ (Milne et al. 1989), which is a typical value of shell-type SNRs in the radio region. No optical emission has been detected from Kes 27 (van den Bergh 1978; Kirshner, Winkler 1979).

The X-ray observation of Kes 27 was initially motivated by the fact that the remnant was located within the error circle of the COS B unidentified γ-ray source, CG327–0 (Hermsen et al. 1977). Lamb and Markert (1981) observed Kes 27 with the Einstein IPC, and found that the X-ray emission was centrally peaked. An IPC image was also given by Seward (1990), which clearly showed clumpy X-ray emission. Seward et al. (1996) reported using ROSAT data that there were several unresolved point-like sources as well as diffuse emission. It showed not

only emission from inside, but also that from the bright eastern shell, which coincides with the bright radio emission. Spectral studies of the diffuse emission showed little difference between the central region and the eastern rim.

We report here on an observation of Kes 27 using the ASCA satellite to study its X-ray structure, particularly its spectral variation.

2.   Observations

The ASCA observation of Kes 27 was performed on 1994 August 21−22. We retrieved these data from DARTS Astrophysical Database at the ISAS PLAIN center. The SISs (Yamashita et al. 1997) were operated in a combination of the 2-CCD BRIGHT mode and of the 4-CCD FAINT mode. Some data were obtained in the 2-CCD mode, while others were obtained in the 4-CCD mode. Since the radio shell of Kes 27 has the diameter of $\sim 20'$, most of the remnant can be covered by the field of view (fov) of the SIS in the 4-CCD mode, which is a square of $22' \times 22'$. Since the major part of the observation was done in the 4-CCD mode, we only selected the 4-CCD FAINT mode data. We excluded all of the data taken at an elevation angle from the Earth rim below 5° from the night Earth rim and 40° (SIS 0) or 20° (SIS 1) from the day Earth rim, a geomagnetic cutoff rigidity lower than 6 GV, and the region of the South Atlantic Anomaly. After screening the above criteria, we further removed the time region of a sudden change of the corner pixels of X-ray events. We then removed the hot and flickering pixels and corrected CTI, DFE and Echo effects (Dotani et al. 1995) from our data set. The exposure times after the screening were 9 ks for SIS 0, and 11 ks for SIS 1. The GISs were operated in the PH mode with the standard bit assignments (Makishima et al. 1996). The GIS data were also screened in a different way. We excluded all of the data taken at an elevation angle from the Earth rim below 5°, a geomagnetic cutoff rigidity lower than 6 GV, and the region of the South Atlantic Anomaly. The exposure times after the screening were 13 ks for GIS 2 and GIS 3, respectively.

3.   Analysis and Results

3.1.   GIS Images

We subtracted the non-X-ray background and the cosmic X-ray background from the data. We then made a correction for vignetting. Figure 1 shows the GIS image of Kes 27 in the 0.7–10 keV energy band. The overlaid contours are the radio map reproduced from the Molonglo Observatory Synthesis Telescope (MOST) observation (Milne et al. 1985, 1989). It clearly shows the centrally peaked X-ray emission confined by the radio shell. In the radio map, there are two bright regions drawn in red contour: one is the east rim and the other is the center. Therefore, the radio-bright rim in the east is relatively dim in X-rays, while the radio-bright center is bright in X-rays.

Figure 2 shows GIS images for two energy bands: the low-energy (0.7–2 keV) band and the high-energy (2–10 keV) band. Comparing the low-energy band image with that obtained by the PSPC (Seward et al. 1996), we noticed that the ASCA image shows no rim brightening in the eastern rim. The eastern rim was detected with the Einstein IPC with relatively weak intensity (Seward 1990). Considering the difference in the energy bands of these detectors, the emission from the eastern rim must be soft in the spectrum.

Seward et al. (1996) reported several point-like X-ray sources detected by the PSPC inside the remnant. Comparing the image obtained by the HRI, they found that these sources show soft emission. Due to the spatial resolution of ASCA, we found no point-like feature corresponding to them. The ASCA image shows a centrally peaked structure that does not coincide with the point source reported.

We generated the GIS band ratio map by dividing the 2–10 keV image by the 0.7–2 keV image, as shown in figure 3. It shows that the central part shows a harder spectrum than that of the outer region. The hardest region statistically coincides with the X-ray brightest region, which might suggest the existence of a point source in the center.

3.2. Spectral Analysis

We extracted the GIS and SIS spectra from the circular region with a diameter of $18'$, which is shown by the outermost circle in the thick solid line in figure 4, which surely covers the entire X-ray emission observed. Since Kes 27 is located near the Galactic plane, $(l, b) = (327°4, +0°4)$, the Galactic ridge emission should be taken into account. Therefore, we extracted the annular region around the source as the background spectra. We selected the annular region of inner and outer diameters of $24'$ and $30'$ as the background for the GIS data. Similarly, we selected the region of the SIS fov outside a circle of $22'$ diameter as background for the SIS data. In the subtraction process, we took into account the vignetting effect of the X-ray optics. After background subtraction, we found that there is no emission above 4 keV. We, therefore, employed the spectra up to 4 keV for a spectral analysis.

We performed a simultaneous fit of the model using the GIS and SIS data. From the spectra in figure 5, the emission lines of Si and S are clearly seen, which indicates that the X-ray emission comes from a thin thermal plasma in origin. We employed the VMEKAL model in FTOOL 5.1 where the free parameters were the interstellar absorption feature, $N_{\rm H}$, electron temperature, $kT_{\rm e}$, abundances of Mg, Si, S, Ar, and Fe. The other metal abundances were fixed to the solar values. We obtained a statistically good fit, the results of which are listed in table 1, of the entire region. The best-fit curves are also shown in figure 5. We should note that the obtained abundances are statistically consistent with those of the solar values. In the spectral fitting, we need not require to employ a model with the non-equilibrium ionization (NEI) condition. The ionization parameter, τ, the product of the electron density and the elapsed time after the shock heating, is longer than $10^{12}\,{\rm cm^{-3}s}$, which indicates that the plasma almost

4

reaches the collisional ionization equilibrium (CIE) condition. Using the plasma density, the value of τ gives us an age estimate of longer than 8×10^4 yr, suggesting that the SNR is in the radiative stage.

We then tried to search for a spectral variation across the remnant. Since the X-ray band ratio map shows a point symmetric structure, we divided the image into two regions: an inner region and an outer region. The inner region has a diameter of $6'$ centered on the intensity peak in figure 4. The outer region has an $18'$ diameter. Figure 6 shows the spectra obtained from the two regions. We also performed a model fitting by employing the same model to that employed for the entire region. The best-fit parameters are given in table 1 as well as the best-fit curves in figure 6. We can notice that most of them show statistically the same value, with the exception of kT_e. We can say that there is a temperature decrease from the inner region towards the outer region that causes the harder spectra in the center.

As we mentioned before, the X-ray brightest region does not coincide with the point source detected by ROSAT. If there is a point source inside the SNR, it usually shows a hard spectrum and a possible pulsation. Seward et al. (1996) noticed the possibility that enhanced central emission could be due to a synchrotron nebula. Our results do not require a power-law type component, like that expected for a possible point source inside the SNR. We picked up photons in the 2–10 keV range of the GIS from the inner region. The total number of photons was 381 with a time resolution of 62.5 ms. A Fourier analysis showed no prominent pulsation component between 0.125–2000 s. Due to the poor statistics, we could not obtain a meaningful upper limit for the pulsation. The origin of the central emission is still unknown.

4. Discussion

4.1. Properties of Kes 27

So far, there is no reliable distance estimate to Kes 27. Seward et al. (1996) assigned a distance of 6.5 kpc by comparing the column density with that of the neighboring SNR, RCW 103 (5° away from Kes 27), whose distance was determined by a H I measurement. Case and Bhattacharya (1998) used a refined Σ–D relation to derive a distance of 4.0 kpc. Here, we adopt a distance of 5 kpc, an intermediate value of two estimates.

In order to determine the extent of the X-ray emitting plasma, we measured the solid angle subtended by a half-maximum intensity contour. In figure 4, the half-maximum intensity contour is drawn by the curved red line. The solid angle subtended by this contour corresponds to a circle with a diameter of $11'.5$. Since Kes 27 shows a filled-center structure with a point-symmetric shape, we assume that the X-ray emitting plasma occupies a sphere with diameter d and a uniform density. If this is the case, the half-maximum intensity contour becomes a circle with a diameter of $\frac{\sqrt{3}}{2}d$. Therefore, we calculated various parameters while assuming the diameter of the plasma to be $13'$ with a uniform density. We also assumed the electron density,

5

n_e, to be equal to the proton density, n_H, for simplicity. These are summarized in table 2.

vWe performed a similar image analysis using the ROSAT PSPC. We found that the solid angle subtended by the half-maximum intensity contour is equal to a circle with a diameter of $12'$, which is almost equal to that by using the ASCA GIS. This can be understood because Kes 27 has such a high N_H that the emission is confined to only the ASCA energy range.

The apparent size in the radio region is $23' \times 19'$ (Whiteoak, Green 1996), which is bigger by 50% in size than that we measured in the X-ray region. The density given in table 2 is that of the X-ray emitting plasma. The total mass in the X-ray emitting region is a part of the mass affected by the SN explosion. The radio-bright region outside the X-ray emitting region must have a higher density than that inside, since it cools down and becomes X-ray dim. Judging from the apparent sizes in the radio and X-ray regions, the total mass occupied outside the X-ray bright region must be by at least one order magnitude bigger than that in the X-ray bright region. Therefore, if the ejecta contain plenty of metal, it must be dissolved into the ISM, resulting in the solar abundance. This shows that Kes 27 is a typical MM SNR.

4.2. Spectral Variation

In the radio band, Kes 27 shows a bright structure along the eastern rim. The bright radio feature on one side of the remnant resembles the radio morphology of SNRs that are known to show an interaction with the molecular cloud, such as 3C 391 and W 44. In general, a detection of shock-excited OH maser emission is a strong evidence for an interaction with the molecular cloud. The detection of OH maser emission was reported for 3C 391 (Frail et al. 1996) and W 44 (Claussen et al. 1997 and references therein), while no OH emission has been detected toward Kes 27 (Frail et al. 1996). Therefore, Rho and Petre (1998) noted that there is no evidence of an actual interaction with the molecular cloud in Kes 27.

The ASCA observation verified the centrally peaked and thin thermal X-ray nature for Kes 27. In addition, we first found a spectral variation from the inner region towards the outer region. It should be noted that the harder spectrum in the inner region comes not from the heavier interstellar absorption but from the higher temperature. The value of kT_e in the inner region is higher by 40% than that in the outer region, while there is no variation of the abundances of heavy elements from a statistical point of view. The temperature gradient suggests that thermal conduction does not play an important role. However, our analysis may be an oversimplification due to showing an one-temperature model. Other SNRs having both a radio shell and centrally peaked X-ray emission with a thermal nature, like Kes 27, have a uniform temperature distribution. For example, no significant kT_e variation has been found in 3C 400.2 (Yoshita et al. 2001), G69.4+1.2 (Yoshita et al. 2000).

As mentioned in subsection 3.1, there are two radio-bright regions in Kes 27: one is in the east rim and the other is in the center. The bright-radio features are generally seen in the rim of the SNR where the matter is compressed by a blast wave. When the matter is

compressed, the polarization becomes prominent. The polarization map given by Milne et al. (1989) shows strong polarization in the east rim as well as in the center where both regions are radio-bright. However, the east rim is X-ray dim and the center is X-ray bright. Therefore, it must be a projection effect that the bright radio feature in the center coincides with the X-ray bright region. Future X-ray observations with a higher spatial resolution, such as by using Chandra or XMM-Newton, will reveal the relation between the X-ray intensity peak and the radio emission.

5. Conclusion

We observed Kes 27, a proto-typical MM SNR, using ASCA GIS and SIS data. We confirmed a filled-center structure in the X-ray region with an angular diameter of $13'$, which is about 50% smaller than that of the radio bright region. The X-ray spectrum can be well fitted by a CIE (VMEKAL) model with solar abundances. Comparing the spectrum from the inner region with that from the outer region, all of the spectral parameters are consistent with each other, with an exception of kT_e. The inner region clearly shows a higher value of kT_e by 40% than that in the outer region. This suggests that the thermal conduction does not play an important role. Our analysis using ASCA supports that Kes 27 is a proto-typical MM SNR.

There are two radio-bright regions in Kes 27: one is in the east rim and the other is in the center. The east rim is X-ray dim while the center is X-ray bright. By taking into account the radio polarization, the coincidence between the X-ray and the radio in the center is found to be a projection effect. A finer observation in the future will reveal the detailed structure in the X-ray region as well as any coincidence between the X-ray and radio regions.

References

[Case(1998)] Case, G. L., & Bhattacharya, D. 1998, ApJ, 504, 761

[Chevalier(1999)] Chevalier, R. A. 1999, ApJ, 511, 798

[Claussen et al.(1997)] Claussen, M. J., Frail, D. A., Goss, W. M., & Gaume, R. A. 1997, ApJ, 489, 143

[Cox(1972)] Cox, D. P. 1972, ApJ, 178, 159

[Dotani et al.(1995)] Dotani, T., Yamashita, A., Rasmussen, A., & the SIS team 1995, ASCA News, 3, 25

[Frail et al.(1996)] Frail, D. A., Goss, W. M., Reynoso, E. M., Giacani, E. B., Green, A. J., & Otrupcek, R. 1996, AJ, 111, 1651

[Hermsen et al.(1977)] Hermsen, W. Swanenburg, B. N., Bignami, G. F., Boella, G., Buccheri, R.,

Scarsi, L., Kanbach, G., Mayer-Hasselwander, H. A., Masnou, J. L., & Paul, J. A. 1977, Nature, 269, 494

[Hwang et al.(2000)] Hwang, U., Holt, S. S., & Petre, R. 2000, ApJ, 537, L119

[Kirshner and Winkler(1979)] Kirshner, R. P., & Winkler, P. F.,Jr. 1979, ApJ, 227, 853

[Lamb and Market(1981)] Lamb, R. C., & Market, T. H. 1981, ApJ, 244, 94

[Makishima et al.(1996)] Makishima, K., Tashiro, M., Ebisawa, K., Ezawa, H., Fukazawa, Y., Gunji, S., Hirayama, M., Idesawa, E., et al. 1996, PASJ, 48, 171

[Milne et al.(1985)] Milne, D. K., Caswell, J. L., Haynes, R. F., Kesteven, M. J., Wellington, K. J., Roger, R. S., & Bunton, J. D. 1985, Proc. Astron. Soc. Australia, 6, 78

[Milne et al.(1989)] Milne, D. K., Caswell, J. L., Kesteven, M. J., Haynes, R. F., & Roger, R. S. 1989, Proc. Astron. Soc. Australia, 8, 187

[Miyata and Tsunemi(1999)] Miyata, E., & Tsunemi, H. 1999 ApJ, 525, 305

[Miyata et al.(1998)] Miyata, E., Tsunemi, H., Kohmura, T., Suzuki, S., & Kumagai, S. 1998, PASJ, 50, 257

[Rho and Petre(1998)] Rho, J., & Petre, R. 1998, ApJ, 503, L167

[Seward(1990)] Seward, F. D. 1990, ApJS, 73, 781

[Seward et al.(1996)] Seward, F. D., Kearns, K. E., & Rhode, K. L. 1996, ApJ, 471, 887

[Bergh(1978)] van den Bergh, S. 1978, ApJS, 38, 119

[White and Long] White, R. L., & Long, K. S. 1991, ApJ, 373, 543

[Whiteoak and Green(1996)] Whiteoak, J. B. Z, & Green, A. J. 1996, A&AS, 118, 329

[Yamashita et al.(1997)] Yamashita, A., Dotani, T., Bautz, M., Crew, G., Ezuka, H., Gendreau, K., Kotani, T., Mitsuda, K., et al. 1997, IEEE Trans. Nucl. Sci., 44, 847

[Yosita et al.(2000)] Yoshita, K., Miyata, E., & Tsunemi, H. 2000, PASJ, 52, 867

[Yosita et al.(2001)] Yoshita, K., Tsunemi, H., Miyata, E., & Mori, K. 2001, PASJ, 53, 93

Table 1. Spectral-fit parameters for Kes 27 in various regions.

Parameter	Entire	Inner	Outer
$N_{\rm H}[10^{22}\,{\rm cm}^{-2}]$	$2.4^{+0.3}_{-0.2}$	2.2 ± 0.3	$2.6^{+0.4}_{-0.3}$
$kT_{\rm e}[{\rm keV}]$	$0.71^{+0.04}_{-0.06}$	0.84 ± 0.08	$0.59^{+0.04}_{-0.06}$
Mg	$1.1^{+0.6}_{-0.3}$	<1.0	$1.1^{+0.9}_{-0.4}$
Si	0.9 ± 0.2	$0.9^{+0.6}_{-0.3}$	0.7 ± 0.2
S	1.1 ± 0.2	$1.2^{+0.6}_{-0.5}$	0.9 ± 0.3
Ar	<1.7	<1.8	<2.1
Fe	$1.2^{+1.1}_{-0.5}$	$1.5^{+1.5}_{-0.9}$	$0.9^{+1.9}_{-0.5}$
χ^2/d.o.f.	$333/342$	$102/90$	$339/280$

Note. Other elements are fixted to those of solar values.

Errors are the 90% confidence level.

Table 2. Physical parameters of Kes 27.

| Parameter	Value
Diameter [pc]	$18.9 d_5$
Temperature [keV] ..	$0.71^{+0.04}_{-0.06}$
Density [cm^{-3}]	$0.39^{+0.03}_{-0.02}\,d_5^{-1/2}$
Thermal energy [erg]	$(1.4\pm0.1)\times10^{50}\,d_5^{5/2}$
Total Mass [$M_\odot$] ...	$34^{+3}_{-2}\,d_5^{5/2}$

Note. d_5 is the distance in units of 5 kpc.
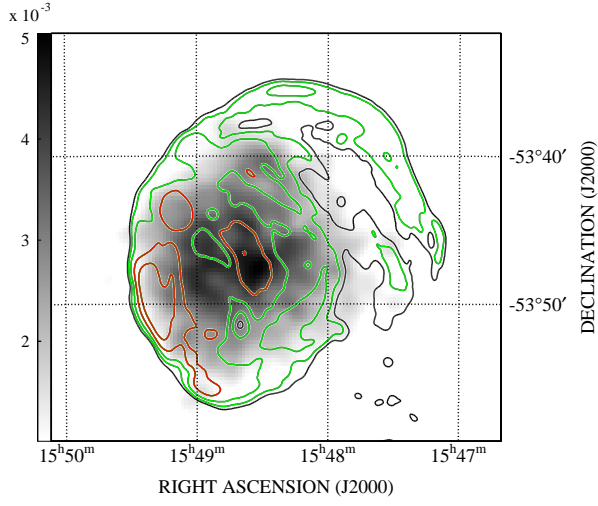
Fig. 1. GIS image in the 0.7−10 keV band overlaid on the MOST contours. The MOST data were retrieved from the on-line version of the MOST Supernova Remnant Catalogue at ⟨http://www.physics.usyd.edu.au/astrop/wg96cat/⟩ (Whiteoak, Green 1996). Radio contours are logalismically spaced (Red, Green, and Black): red is the strongest, followed by green and black.
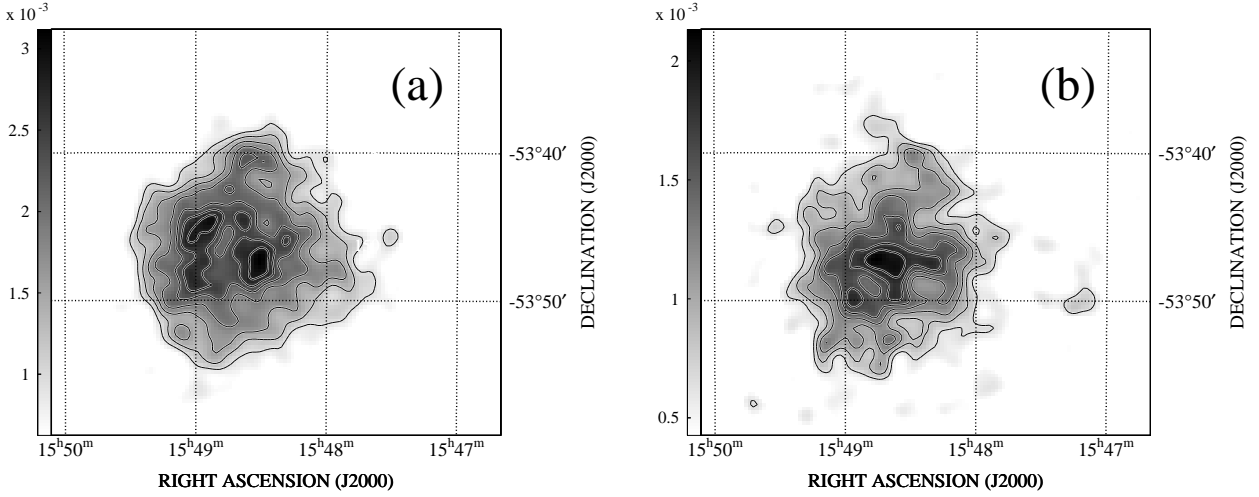

Fig. 2. Same as for figure 1 for the 0.7–2 keV band (a) and for the 2–10 keV band (b). The contours are linearly spaced X-ray intensity.

10
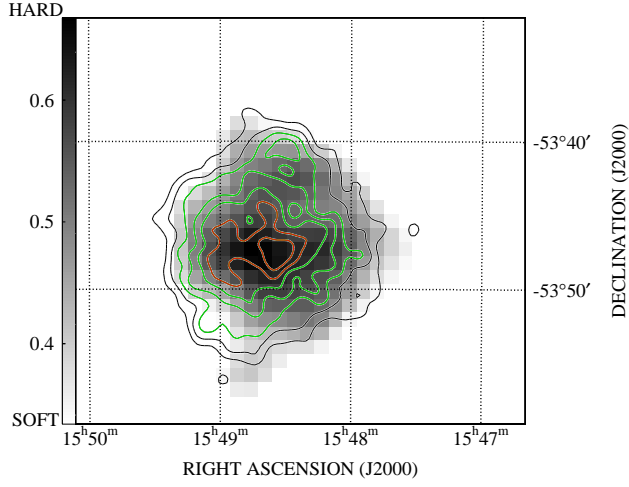
Fig. 3. GIS band ratio map (2–10 keV/0.7–2 keV). The contours shows the X-ray intensity (0.7–10 keV), as shown in figure 1: red is the strongest, followed by green and black.
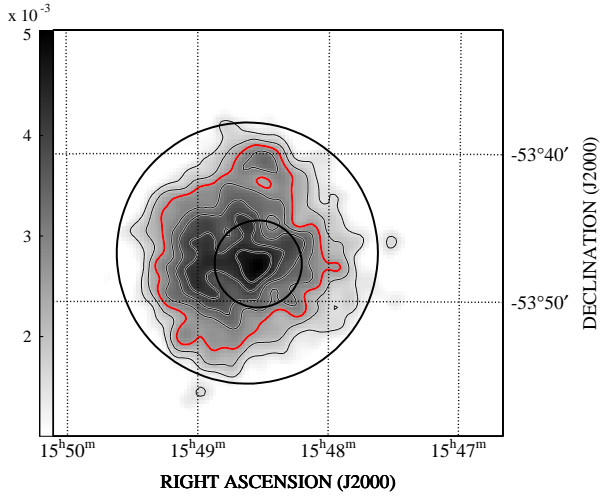
Fig. 4. ASCA GIS image in the energy range 0.7–10 keV. The gray-scale bar is in units of count s^{-1} arcmin^{-2}. The contour values are linearly spaced from 0.3 to 0.9 of the peak surface brightness. The circles in the solid line indicate the regions used for the spectral analysis. The half-maximum intensity is also drawn by the thick red solid contour.

11
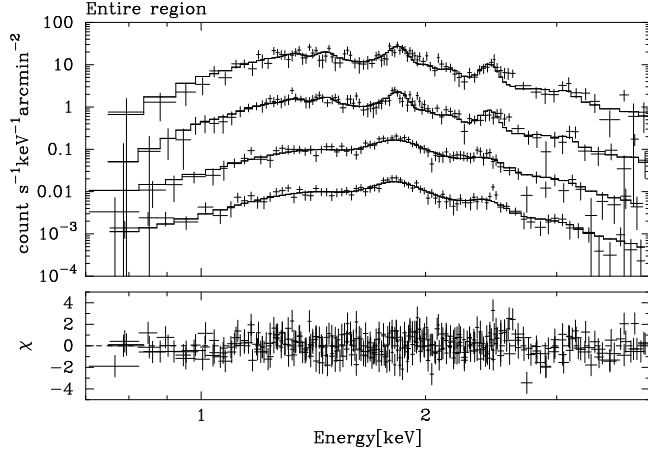
Fig. 5. Spectra from the entire region of Kes 27. Best-fit VMEKAL models are shown by the solid lines. The spectra correspond to SIS 0 (× 100), SIS 1 (× 10), GIS 2, and GIS 3 (× 0.1) from top to bottom. The lower panel shows the residuals.
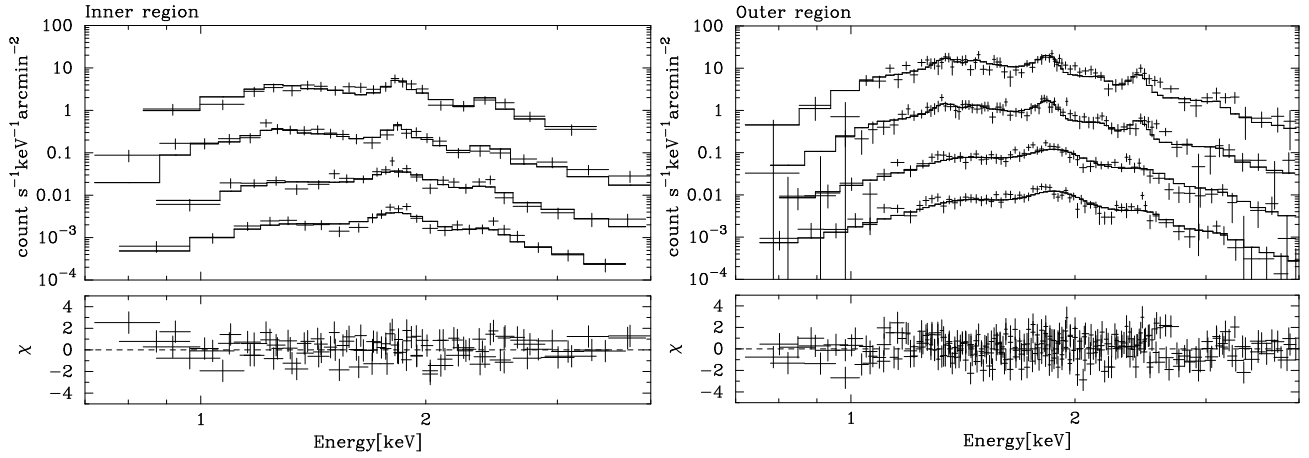
Fig. 6. Same as figure 5, but for the inner region (left) and the outer region (right).